M. Donoghue

R. Stevenson
Advanced Engineering Staff,
General Motors Technical Center,
Warren, Mich. 48090-9040

Y. J. Kwon

N. Triantafyllidis
Department of Aerospace Engineering,
The University of Michigan,
Ann Arbor, Michigan 48109-2140

An Experimental Verification of the Hemispherical Cup Puckering Problem

In this work is presented an experimental study of the hemispherical cup puckering test. This investigation is motivated by some theoretical as well as by some practical reasons which are elaborated upon in the introduction. After a brief outline of the analytical model and the corresponding numerical solution technique, the presentation continues with a description of the experimental procedure. A comparison between the experimental and the theoretical results is given next followed by a critical discussion.

1 Introduction

An interesting plastic instability phenomenon, which, in spite of its practical importance in sheet metal forming applications, has received little attention thus far, is the so-called "puckering" phenomenon. The earliest reference to this problem in the literature appears to be in the book by Devons (1941), where puckering is defined as the waviness formed in that part of the (usually curved) wall of a drawn shape that has already passed over the radius of the die (as opposed to wrinkling, which is the term used for the formation of corrugations in the flat part of the blank, which has not yet passed over the die radius).

The specific problem to be investigated here is the plastic bifurcation of an initially flat circular plate held between a blankholder and a die, and axisymmetrically deformed by a spherically shaped punch as shown in Fig. 1. Since material can flow inwards from the outer flange to the cup's wall, compressive hoop stresses are developed at the contact-free part of the shell, which upon attaining a critical level, induce a nonaxisymmetric bifurcation.

The motivation for the present experimental investigation is twofold. On the theoretical side the problem possesses the very interesting (and only recently investigated, see Triantafyllidis (1983), Nguyen and Triantafyllidis (1989) for more details) feature of strong deviations from proportional loading in the prebifucation solution, thus making a smooth bifurcation possible. On the practical side, the puckering of the hemispherical cup can serve as a simple but realistic model for surface waviness instabilities occuring during complex sheet metal forming operations. A consistent and general instability criterion for such problems, not requiring the consideration of a nonlinear shell theory, which is necessary for the classical analysis of this type problems, has been developed in Triantafyllidis and Kwon (1987), and the present set of experiments provides a very good test case for the checking of aforementioned general theory.

Although the theoretical model for the present experiments has been presented in a previous paper by Triantafyllidis (1985), for reasons of completeness of the presentation as well as in view of some differences with the analysis in Triantafyllidis (1985) (mainly the inclusion of - the experimentally inevitable - friction into the model), a brief description of the theoretical model is presented in this work. Thus, Section 2 is devoted to the description of the prebifurcation solution, the bifurcation analysis and the corresponding numerical solution. In Section 3 the experimental procedures are described, while in Section 4 the experimental results are compared with the theoretical predictions. The presentation is concluded by a critical review of the results discussed in Section 4.

2 Theoretical Formulation

A detailed derivation of the model for the onset of a puckering instability in the hemispherical cup test has already been

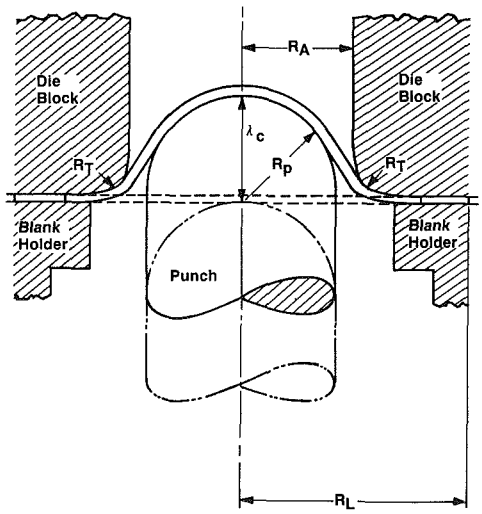

Fig. 1 Schematic drawing of the punch test, (— — — —) initial stress free configuration; (———) final configuration

Contributed by the Materials Division for publication in the JOURNAL OF ENGINEERING MATERIALS AND TECHNOLOGY. Manuscript received by the Materials Division January 14, 1988.

presented in Triantafyllidis (1985). However, in view of some additional complications in the experiments reported here (mainly the presence of friction which is ignored in the aforementioned reference), as well as for the completeness of the presentation, a brief description of the theoretical model is included here.

2.1 Prebifurcation Solution. Consider an initially flat circular disk of uniform thickness H and radius R_L. The plate is held between a die block of aperture radius R_A, and a blankholder of aperature radius $R_B = R_A + R_T$, where R_T is the cross sectional radius of the die's throat, as depicted in Fig. 1. A hemispherical punch of radius $R_P (R_P \leq R_A)$ pushes the plate from its initial (flat) stress-free configuration into a deformed shape as shown in Fig. 1. Moreover, λ denotes the total punch travel from the initial configuration, and serves as the time like parameter in this problem, since it increases monotonically during the test.

For reasons to be subsequently elaborated upon, only the axisymmetric membrane stresses of the prebifurcated solution are required to determine the onset of the asymmetric puckering instability. A full Lagrangian description of the weak form of the equilibrium equations (i.e. principle of virtual work) for the axisymmetric membrane is adopted here with the initial stress free configuration taken to be the reference one. If $u(r)$ and $w(r)$ are the horizontal and vertical displacements, respectively, of a material point initially at a distance r from the plate's center, the internal virtual work (per radian) of the plate is

$$\text{I.V.W.} = \int_0^{R_L} [(r+u)\sigma_r \delta(\lambda_r) + \lambda_r r \sigma_\theta \delta(\lambda_\theta)] h dr \tag{2.1}$$

where σ_r, σ_θ are the radial and circumferential Cauchy stresses, h is the current sheet thickness and λ_r, λ_θ are the radial and circumferential stretch ratios given by:

$$\lambda_r = [(1+du/dr)^2 + (dw/dr)^2]^{1/2}, \quad \lambda_\theta = 1 + u/r \tag{2.2}$$

The external virtual work term consists of two parts. The first part is due to the contact between the sheet and the punch, blankholder/die assembly and is taken to be

$$(\text{E.V.W.})_c = -\delta\left\{\frac{k}{2}\int_0^{R_L} [(d_1)^2 H(d_1) + (d_2)^2 H(d_2) + 2(w-w_0)^2 H(r+u-R_B)] r dr\right\} \tag{2.3}$$

where d_1, d_2, w are, respectively, the (small) penetration distances of the sheet on the hemispherical punch, the curved and the flat part of the die. In addition, k denotes the foundation stiffness, $H(x)$ designates the Heaviside function ($H(x)=0$ if $x<0$, $H(x)=1$ if $x \geq 0$), while w_0 is the initial penetration of the sheet into the die block due to the applied blankholder load $P_R = 2\pi k(R_L{}^2 - R_B{}^2)w_0$. Moreover, the punch and die throat penetration distances d_1 and d_2 are given by:

$$d_1 = R_P - [(r+u)^2 + (w - w_0 + R_P - \lambda)^2]^{1/2},$$
$$d_2 = R_T - [(r+u-R_B)^2 + (R_T - w + w_0)^2]^{1/2} \tag{2.4}$$

The second part of the external virtual work is due to friction. A slightly modified version of Coulomb's law that has been used in Triantafyllidis and Maker (1986), will be adopted. In this law, the friction coefficient depends on the total sliding distance u_T of the point of the sheet in question on the rigid surface it contacts, and is equal to $\mu f(u_T)$*, where $f(u_T)$ is a monotonically increasing function of u_T with $f(0)=0$ and $f(\infty)=1$. The function f is chosen to reach a value very close to unity shortly after the sliding contact starts, i.e. for a small value of u_T; typically the friction coefficient is developed at 99 percent for $u_T = 0.01H$. Hence, the friction part of the external virtual work is assumed to be

$$(\text{E.V.W.})_f = \mu k\left\{\int_0^{R_L} [d_1 H(d_1) f_1(\mathbf{t}_1 \cdot \delta\mathbf{u}) + d_2 H(d_2) f_2(\mathbf{t}_2 \cdot \delta\mathbf{u}) + 2wH(r+u-R_B)(\mathbf{t}\cdot\delta\mathbf{u})] r dr\right\} \tag{2.5}$$

where $\mathbf{t}_1$, $\mathbf{t}_2$ and $\mathbf{t}$ are the unit tangent vectors on the hemispherical punch surface, the die throat surface and the flat surface of the die, respectively. It should be mentioned here that the factor of two appearing in front of the third term in (2.4) and (2.5) is due to the fact that both the upper and lower parts of the blankholder/die assembly are in contact with the sheet. Hence, the weak formulation of the membrane equilibrium equations is

$$(\text{I.V.W.}) = (\text{E.V.W.})_c + (\text{E.V.W.})_f \tag{2.6}$$

At this point, the constitutive equation for the solid is introduced. As discussed in Triantafyllidis (1985), due to the presence of unloading in the principal branch of the solution, the phenomenological corner type model introduced by Christofferson and Hutchinson (1979) is employed here. The aforementioned model, which is a rate independent plasticity model, has a stress rate potential given by

$$W = \frac{1}{2} \overset{\nabla}{\tau}_{ij} (M_{ijkl} + g(\theta) C_{ijkl}) \overset{\nabla}{\tau}_{kl} \tag{2.7}$$

where $\overset{\nabla}{\tau}_{ij}$ is the Jaumann rate of Kirchhoff stress, M_{ijkl} is the linear elastic compliance tensor

$$M_{ijkl} = \frac{1+\nu}{\mathrm{E}}\left[\frac{1}{2}(\delta_{ik}\delta_{jl} + \delta_{il}\delta_{jk}) - \frac{\nu}{1+\nu}\delta_{ij}\delta_{kl}\right\rangle \tag{2.8}$$

and C_{ijkl} is the total plastic compliance tensor with

$$C_{ijkl} = \left(\frac{1}{\mathrm{E}_s} - \frac{1}{\mathrm{E}}\right)\frac{\partial^2 \phi}{\partial \tau_{ij}\partial \tau_{kl}} + \frac{1}{2\phi}\left(\frac{1}{\mathrm{E}_t} - \frac{1}{\mathrm{E}_s}\right)\frac{\partial \phi}{\partial \tau_{ij}}\frac{\partial \phi}{\partial \tau_{kl}}$$
$$\tau_e^2 = 2\phi = [(\tau_{11}-\tau_{33})^2 + (\tau_{22}-\tau_{33})^2 + R(\tau_{11}-\tau_{22})^2 + 2(1+2R)(\tau_{12})^2]/(1+R) \tag{2.9}$$

Here τ_e is the material's equivalent stress, E_s and E_t are the secant and tangent moduli of the uniaxial stress-strain curve, E is the Young's modulus, ν the Poisson's ratio, and R the material's transverse anisotropy ratio (it is tacitly assumed that the sheet is isotropic in its own plane, but it can be transversely anisotropic in the thickness direction). Moreover, the material's transition function $g(\theta)$ is assumed to be (see Christoffersen and Hutchinson (1979))

$$g(\theta) = \begin{cases} 1 & \text{for } 0 \leq \theta \leq \theta_0 \\ \cos^2[0.5\pi(\theta-\theta_0)/(\theta_c-\theta_0)] & \text{for } \theta_0 \leq \theta \leq \theta_c \\ 0 & \text{for } \theta_c \leq \theta \leq \pi \end{cases} \tag{2.10}$$

where θ is the angular deviation (in stress-rate space) from proportional loading and is defined by

$$\cos\theta = \tau_{ij} C_{ijkl} \overset{\nabla}{\tau}_{kl} / [(\tau_{mn} C_{mnrs} \tau_{rs})(\overset{\nabla}{\tau}_{pq} C_{pquv} \overset{\nabla}{\tau}_{uv})]^{1/2} \tag{2.11}$$

Using (2.7), the incremental form of the material's constitutive equation is

$$\dot{E}_{ij} = \partial W / \partial \overset{\nabla}{\tau}_{ij} = (\partial^2 W / \partial \tau_{ij} \partial \tau_{kl}) \overset{\nabla}{\tau}_{kl} \tag{2.12}$$

where the term in parenthesis is the material's compliance tensor, i.e. the inverse of its incremental moduli tensor. ($L_{ijkl} = (\partial^2 W / \partial \tau_{ij} \partial \tau_{kl})^{-1}$)

The aforedescribed constitutive equation for the material, in conjunction with the rate form of the equilibrium equation (2.6) will furnish the prebifurcation solution to the problem

*Note: It is tacitly assumed that no sliding direction reversals occur, a condition which is always satisfied in this problem.

via a f.e.m. (finite element method) technique, as it will be explained in the appropriate section.

One should also mention at this point that the only nonzero stresses are the membrane plane stresses in the radial and hoop directions, which are calculated by inverting (2.12) after also taking into account the plane stress approximation ($\overset{\nabla}{\tau}_{33} = \tau_{33} = 0$).

2.2 Bifurcation Analysis. Following Triantafyllidis (1985), the onset of a puckering instability is detected by the loss of positive definitness of the bifurcation functional

$$F(\lambda;\, \bar{u},\, \bar{v},\, \bar{w}) = 2\pi[F_0(\lambda;u_0',\, 0,\, w_0') + F_0(\lambda;0,\, v_0,\, 0)] +$$

$$\pi \sum_{n=1}^{\infty} [F_n(\lambda;u_n,\, v_n,\, w_n) + F_n(\lambda;u_n',\, v_n',\, w_n')] \qquad (2.13)$$

where u_n, v_n, w_n, u_n', v_n', w_n' are the Fourier series amplitudes of the admissible functions $\bar{u}$, $\bar{v}$, $\bar{w}$, namely the two tangential and the normal components of the bifurcation amplitude, i.e.

$$\bar{u}(r,\theta) = \sum_{n=0}^{\infty} [u_n'(r)\cos(n\theta) + u_n(r)\sin(n\theta)]$$

$$\bar{v}(r,\theta) = \sum_{n=0}^{\infty} [v_n(r)\cos(n\theta) + v_n'(r)\sin(n\theta)] \qquad (2.14)$$

$$\bar{w}(r,\theta) = \sum_{n=0}^{\infty} [w_n'(r)\cos(n\theta) + w_n(r)\sin(n\theta)]$$

Adopting for the sake of notational simplicity u^*, v^*, w^* to stand for either u_n, v_n, w_n or u_n', v_n', w_n', the functional F_n in (2.13) is given by

$$F_n(\lambda;\, u^*,\, v^*,\, w^*) = \int_0^{R_L} \left\{ C_{11}\left[\left(\frac{du^*}{dr} + \lambda_r\kappa_r w^*\right)^2 + \frac{h^2}{12}\left(\frac{d}{dr}\left(\frac{1}{\lambda_r}\frac{dw^*}{dr}\right)\right)^2\right] + \right.$$

$$2C_{12}\left[\left(\frac{du^*}{dr} + \lambda_r\kappa_r w^*\right)(-nv^* + u^*\cos\phi + w^*\sin\phi) + \frac{h^2}{12}\left(\frac{d}{dr}\left(\frac{1}{\lambda_r}\frac{dw^*}{dr}\right)\right)\left(-\frac{n^2}{r+u}w^* + \frac{\cos\phi}{\lambda_r}\frac{dw^*}{dr}\right)\right]$$

$$+ C_{22}\left[(-nv^* + u^*\cos\phi + w^*\sin\phi)^2 + \frac{h^2}{12}\left(-\frac{n^2}{r+u}w^* + \frac{\cos\phi}{\lambda_r}\frac{dw^*}{dr}\right)^2\right] +$$

$$D_{11}\left[\left(\frac{dv^*}{dr}\right)^2 + \frac{h^2}{12}\left(\frac{d}{dr}\left(\frac{nw^*}{r+u}\right)\right)^2\right] + \qquad (2.15)$$

$$2D_{12}\left[\left(\frac{dv^*}{dr}\right)(nu^* - v^*\cos\phi) + \frac{h^2}{12}\left(\frac{d}{dr}\left(\frac{nw^*}{r+u}\right)\right)\left(\frac{n}{\lambda_r}\frac{dw^*}{dr} - \frac{n\cos\phi}{r+u}w^*\right)\right] +$$

$$D_{22}\left[(nu^* - v\cos\phi)^2 + \frac{h^2}{12}\left(\frac{n}{\lambda_r}\frac{dw^*}{dr} - \frac{n\cos\phi}{r+u}w^*\right)^2\right] +$$

$$h\sigma_r\left(\frac{1}{\lambda_r}\frac{dw^*}{dr}\right)^2 + h\sigma_\theta\left(\frac{n}{r+u}w^*\right)^2 + kw^{*2}(H(d_1) + H(d_2) + 2H(r+u-R_B))\Big\}(r+u)\lambda_r dr$$

with

$$C_{11} = h(L_{rrrr} - L_{rrzz}L_{zzrr}/L_{zzzz} - \sigma_r)/\lambda_r^2$$
$$C_{12} = h(L_{rr\theta\theta} - L_{rrzz}L_{zz\theta\theta}/L_{zzzz})/\lambda_r(r+u)$$
$$C_{22} = h(L_{\theta\theta\theta\theta} - L_{\theta\theta zz}L_{zz\theta\theta}/L_{zzzz} - \sigma_\theta)/(r+u)^2 \qquad (2.16)$$
$$D_{11} = h(L_{r\theta r\theta} + (\sigma_r - \sigma_\theta)/2)/\lambda_r^2$$
$$D_{12} = h(L_{r\theta r\theta} - (\sigma_r + \sigma_\theta)/2)/\lambda_r(r+u)$$
$$D_{22} = h(L_{r\theta r\theta} + (\sigma_\theta - \sigma_r)/2)/(r+u)^2$$

where L_{ijkl} in (2.16) are the physical components of the incremental moduli tensor of the material (the inverse of the compliance tensor given in (2.12) with indices 1,2,3 corresponding to the r, θ, z directions, respectively). In addition to the principal stretch ratios λ_r, λ_θ given by (2.2), the principal curvatures κ_r and κ_θ, as well as the angle ϕ formed between the outward normal to the shell's midsurface and its symmetry axis are required, and they can be expressed in terms of the prebifurcation horizontal and vertical displacements $u(r)$ and $w(r)$ by

$$\sin\phi = -(dw/dr)/\lambda_r,\ \cos\phi = (1 + (du/dr))/\lambda_r$$
$$\kappa_r = ((dw/dr)(d^2u/dr^2) - (1 + (du/dr))(d^2w/dr^2))/\lambda_r^3,$$
$$\kappa_\theta = -(dw/dr)/\lambda_r(r+u) \qquad (2.17)$$

Note that F_n is quadratic with respect u^*, v^*, w^*, and is completely specified once the total prebifurcation displacements $u(r)$, $w(r)$, the current thickness $h(r)$, the membrane stresses $\sigma_r(r)$, $\sigma_\theta(r)$ and the current incremental moduli $L_{ijkl}(r)$ are given. The determination of the aforementioned quantities, which depend on the punch advance parameter λ, follows from the prebifurcation analysis of the axisymmetric membrane problem outlined in the previous subsection.

The critical punch height λ_c is then given by the minimum, over all integers n, of the lowest eigenvalue $\hat{\lambda}(n)$ of each functional F_n. The circumferential wavenumber corresponding to the critical punch height λ_c is denoted by n_c. The essential boundary conditions to be imposed on the minimum eigenvalue problem for the functional $F_n(\lambda;\, u^*,\, v^*,\, w^*)$ are the apex conditions $u^* = v^* = w^* = dw^*/dr = 0$ at $r = 0$ for $n \neq 0$ and $u^* = v^* = dw^*/dr = 0$ for $n = 0$.

As discussed in Triantafyllidis (1985), the derivation of the bifurcation functional for the puckering problem takes into account the Kirchhoff-Love hypothesis (i.e., the approximate plane stress condition in the shell and the negligible transverse shear strain assumption) and the shallowness of the eigenmode. The validity of these assumptions, as well as a mathematically more elegant (and consistent) derivation of the bifurcation functional in (2.13) using a multiple scales asymptotic expansion method, is presented in Triantafyllidis and Kwon (1987).

2.3 Numerical Method. The finite element method is employed for the evaluation of the prebifurcation solution of the structure, as well as for the determination of the critical height $\hat{\lambda}(n)$ corresponding to a given wavenumber n.

The basis for the solution algorithm for the principal branch is the incremental virtual work formulation derived from (2.6), namely

$$\Delta\lambda[(\text{I.V.W.})^{\cdot} - (\text{E.V.W.})^{\cdot}] = -(\text{I.V.W.} - \text{E.V.W.}) \qquad (2.18)$$

In the strain-displacement equation (2.2) (see also (2.4)) only spatial derivatives up to the first order of the total displacement components $u(r)$, $w(r)$ are involved. Thus piecewise continuous (C°) shape functions are employed here. Higher order shape functions cannot be used in this case in view of the anticipated shape discontinuities at the points of loss of contact between the membrane and the punch or the die throat. Consequently, the displacements $u(r)$, $w(r)$ are linearly interpolated within each element.

Due to the expected rapid variations of the stress field as well as the loading direction angle θ in the neighborhood of the die throat, the power law type mesh refinement employed in Triantafyllidis (1985) has been adopted

$$|r_n - R_B| = \Delta l\,|(R_B + (\alpha-1)\Delta l - r_0)/\alpha\Delta l|^{\alpha};$$
$$R_B + (2\alpha-1)\Delta l > r_0 > R_B - \Delta l \tag{2.19}$$

where r_n is the new (refined) coordinate and r_0 the one corresponding to a uniform subdivision of the interval $[0,\ R_L + 2(\alpha-1)\Delta l]$. The mesh refinement exponent is denoted by α and the refined zone of the plate extends by Δl on each side of the blankholder radius R_B. In all the calculations reported here $\alpha = 2$, $\Delta l = 1.7R_T$.

An incremental Newton-Raphson algorithm based on (2.18) is adopted for the principal solution. The material used for the experiment was transversely isotropic and thus in all the calculations $R = 1$. As discussed in Triantafyllidis (1985), an $O(10^{-3})$ stress accuracy requirement dictated a step size $\Delta\lambda = 0.1H$. In some calculations $\Delta\lambda = 0.05H$ is also considered with no appreciable difference in the results.

To avoid numerical problems associated with the beginning of the loading process, a slightly deformed stress free shape of the membrane is considered. More specifically, following Triantafyllidis (1985), in the stress free state the initial deviation $w_i(r)$ of a material point r from the planar reference configuration is taken to be

$$w_i(r) = \begin{cases} (R_P^2 - r^2)^{1/2} - R_P + \lambda_i + w_0 \\ \text{for } 0 < r < R_P\sin\beta_i \\ R_T(1-\cos\beta_i) + [R_A + R_T(1-\sin\beta_i) - r]\tan\beta_i + w_0 \\ \text{for } R_P\sin\beta_i < r < R_A + R_T(1-\sin\beta_i) \\ R_T - [R_T^2 + (R_B - r)^2]^{1/2} + w_0 \\ \text{for } R_A + R_T(1-\sin\beta_i) < r < R_B \\ w_0 \text{ for } R_B < r < R_L \end{cases} \tag{2.20}$$

where λ_i is the distance of the apex of the membrane from the flat configuration and $2\beta_i$ is the angle of initial contact between the punch and the membrane. The relation between λ_i and β_i is found from simple geometrical considerations to be

$$\lambda_i = R_P + R_T + [R_B\sin\beta_i - (R_P + R_T)]/\cos\beta_i \tag{2.21}$$

In addition, w_0 is the initial uniform vertical displacement of the plate due to the imposition of the applied blankholder load $P_B = 2\pi k(R_L{}^2 - R_B{}^2)w_0$. For reasons elaborated upon in Triantafyllidis (1985), the initial contact angle is $\beta_i = 0.035$ rad, while the punch stiffness is $k = 0.05\,E/H$ in all the calculations reported here. As far as the mesh employed in the finite element calculations is concerned, the stretched coordinate r_0 (see (2.19)) interval $[0,\ R_L + 2(\alpha-1)\Delta l]$ is divided into equal subintervals of constant size Δr. Following Triantafyllidis (1985), in all the calculations $\Delta r = 0.025R_A$.

The determination of the critical height $\hat{\lambda}(n)$ for a given wavenumber n, requires the investigation of the positive definitness of the functional F_n defined in (2.15), a check which is repeated at every step of the deformation as the punch advance λ increases. A straightforward finite element discretization of F_n is employed, using linear interpolation for u^* and v^* within each element and a Hermitian interpolation for w^*, the choice being dictated by the functional dependence of F_n on u^*, v^*, w^* and their spatial derivatives. The resulting discretized stiffness matrix, say $\mathbf{K}$, is subsequently decomposed using a modified Cholesky decomposition $\mathbf{K} = \mathbf{LDL}^T$, with $\mathbf{L}$ a lower triangular matrix and $\mathbf{D}$ a diagonal matrix. Positive definitness of $\mathbf{K}$ is lost as soon as an entry of $\mathbf{D}$ becomes negative.

Table 1 Tooling dimensions

S_1	S_2	S_3
$R_P = 0.05000$ m	$R_P = 0.03333$ m	$R_P = 0.01666$ m
$R_A = 0.05833$ m	$R_A = 0.03887$ m	$R_A = 0.01945$ m
$R_T = 0.01041$ m	$R_T = 0.00694$ m	$R_T = 0.00347$ m

3 Description of Experiments

The tests reported in this work were performed using a series 866 Metal Forming Analysis System developed by MTS. This system, which can be seen in Plate 1, consists essentially of the axisymmetric punch and blankholder die assembly (also called ring assembly), depicted in the open position in Plate 2, and uses closed loop computer controlled servohydraulics. The inputs to the system are the punch load or velocity and the blankholder (ring) load.

Three sets of tools S_1, S_2, S_3 were machined out of D2 hardened tool steel for the experiments. Each set consisted of a hemispherical punch of radius R_P, an upper ring of aperture radius R_A with cross sectional die throat radius R_T, and a

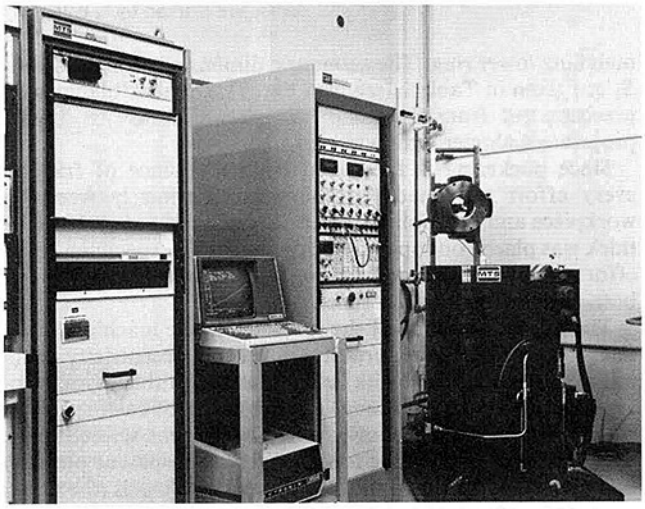

Plate 1 Experimental setup. General view

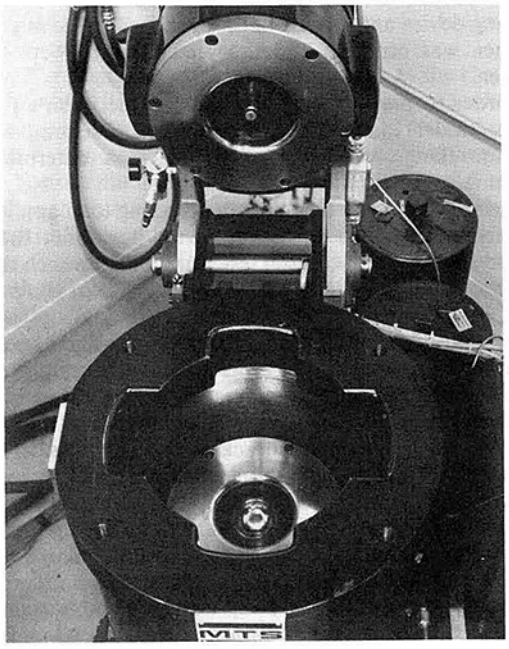

Plate 2 Loading device in its open position

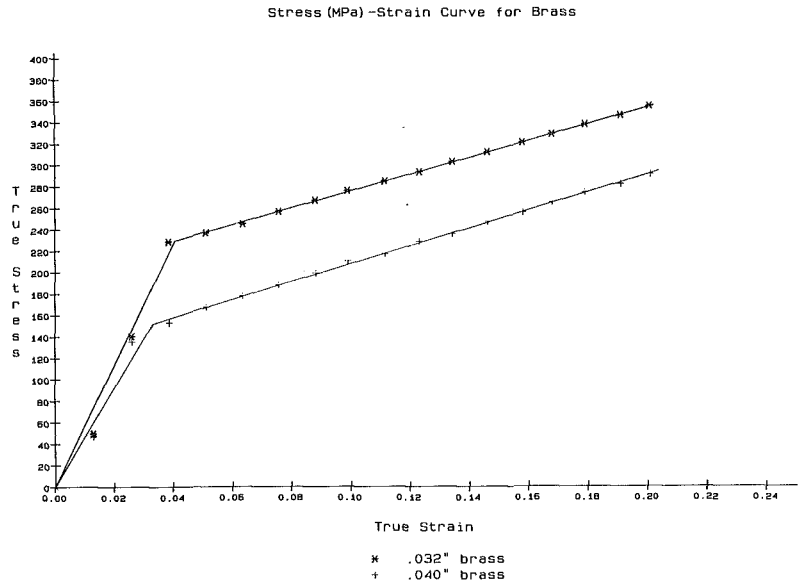

Fig. 2 Uniaxial stress-strain curves for brass: 0.020, 0.025, 0.032 in. curves are marked by *, 0.040 in. curve is marked by +

matching lower ring. The geometric dimensions for S_1, S_2 and S_3 are given in Table 1 (see also Fig. 1). Circular blanks were precision cut from the same flat sheet of brass to the appropriate diameter and deburred.

Since puckering is facilitated by the absence of friction, every effort was made to minimize friction between the workpiece and the tooling. A teflon sheet 0.005 in (0.127 mm) thick was placed on top and bottom of the test specimen. In an effort to further reduce friction, mill oil was also applied to both sides of each teflon sheet.

The proper centering of the specimen in the machine turned out to be extremely important, for a small eccentricity in the initial position of the blank leads to unacceptable asymmetric prebifurcation deformations. The centering of each specimen was accomplished as follows: A cross-hair was scribed at the center of each blank. The tooling had a transparent plexiglas device permitting the location of the machine's axis (the device consisted of two parallel planes perpendicular to the machine's axis of symmetry and each having a cross-hair scribed on its center). Once the three cross-hairs (two of the centering device and one from the specimen) were aligned, the specimen was centered and the binder plates were brought together.

In order to prevent wrinkling on the specimen's flange, a ring (or binder) load P_R had to be applied. The minimum ring load for flange wrinkling avoidance was determined experimentally for each case.

Once the blank was clamped and the ring load applied to it, the punch penetrated the sheet metal beginning the draw. Prior to the initiation of each test a maximum punch displacement was input into the machine. At the end of the punching phase, the test specimen was inspected for any apparent puckering by shining light onto the specimen and also rubbing it with a soft paper cloth in order to feel any asymmetric surface irregularities. Once a dome height was determined at which puckering can be found, the exact critical dome height value for which the onset of puckering occurs was determined by running different test specimens at progressively less dome heights (maximum punch height decrease each time $\Delta H = 0.635$ mm) and checking every time for signs of asymmetric deformation in the unsupported area of the specimen until no such asymmetry could be found.

The material used in the tests was soft tempered brass of 61.5 percent Cu, 35.4 percent Zn and 3.1 percent Pb. The basic mechanical properties of interest, namely the plastic

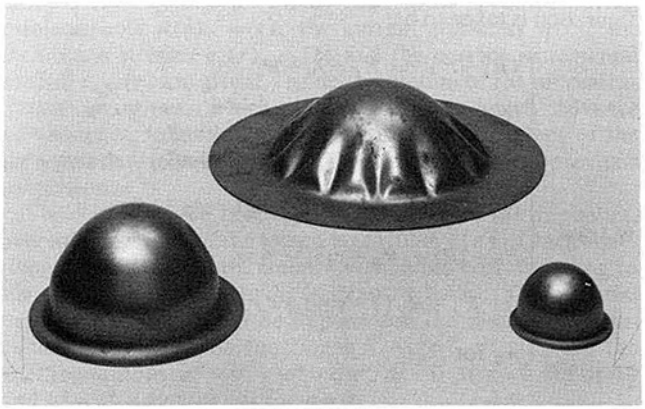

Plate 3 Test specimens corresponding to various stages of deformation: prebuckling state (far right), onset of buckling (far left) and postbuckling state (middle)

anisotropy ratio R and the uniaxial stress-strain curve, were measured and used into the material model described in Section 2.

The sheet's anisotropy ratio was found to be $R = 1$ and did not vary significantly with the change of direction (variations of R at angles of 0, 45, and 90 deg with respect to the rolling direction were of the order 2 percent).

The material's uniaxial stress-strain curve is shown in Fig. 2. Of the four different sheets of brass used in the experiments, the sheets with thicknesses of 0.020 in. (0.508 mm), 0.025 in. (0.635 mm), 0.032 in. (0.813 mm) had the same uniaxial response (marked with * in Fig. 2), while the 0.040 in. (1.016 mm) thick sheet had a different uniaxial stress-strain curve (marked with + in Fig. 2). For computational convenience, the uniaxial stress-strain curve was idealized as a bilinear hardening model, as one can also see in Fig. 2.

Finally, a note about the experimental determination of the critical circumferential wavenumber n_c at the onset of puckering. In view of the aforedescribed experimental determination of the critical dome height, the experimental determination of n_c is very difficult. Assuming no mode jumping in the postbifurcated range of the deformation, i.e., that n_c is also the axial wavenumber of the postbifurcated solution, few experiments were carried well into the postbuckling range and their corresponding n_c were determined. As expected, since n_c is basically a factor depending on geometry (see Triantafyllidis

Table 2

Draw Ratio \ Thickness		$H_1 = 0.508$ mm			$H_2 = 0.635$ mm			$H_3 = 0.813$ mm			$H_4 = 1.016$ mm		
Draw Ratio	Tools	S_1	S_2	S_3	S_1	S_2	S_3	S_1	S_2	S_3	S_1	S_2	S_3
$\frac{R_L}{R_A} = 1.3$		$P_R =$ 46,726 *Nt*	$P_R =$ 56,445 *Nt*	$P_R =$ 45,632 *Nt*	–	$P_R =$ 57,535 *Nt*	$P_R =$ 46,980 *Nt*	–	$P_R =$ 54,865 *Nt*	$P_R =$ 41,316 *Nt*	–	–	$P_R =$ 40,938 *Nt*
$\frac{R_L}{R_A} = 1.5$		$P_R =$ 47,189 *Nt*	$P_R =$ 46,010 *Nt*	$P_R =$ 33,168 *Nt*	–	$P_R =$ 43,434 *Nt*	$P_R =$ 33,373 *Nt*	–	–	$P_R =$ 33,818 *Nt*	–	–	$P_R =$ 41,320 *Nt*
$\frac{R_L}{R_A} = 1.7$		–	$P_R =$ 49,570 *Nt*	$P_R =$ 34,637 *Nt*	–	$P_R =$ 49,837 *Nt*	$P_R =$ 33,809 *Nt*	–	–	$P_R =$ 41,227 *Nt*	–	–	$P_R =$ 41,316 *Nt*

Draw Ratio \ Thickness / Tools	$H_1 = 0.508$ mm			$H_2 = 0.635$ mm			$H_3 = 0.813$ mm			$H_4 = 1.016$ mm		
	S_1	S_2	S_3	S_1	S_2	S_3	S_1	S_2	S_3	S_1	S_2	S_3
$\frac{R_L}{R_A} = 1.3$	$\lambda_c =$ 8.38mm	$\lambda_c =$ 8.38mm	$\lambda_c =$ 7.11mm	NW	$\lambda_c =$ 13.46mm	$\lambda_c =$ 7.87mm	NW	$\lambda_c =$ 23.88mm	$\lambda_c =$ 8.89mm	NW	NW	$\lambda_c =$ 15.24mm
	$\lambda_c =$ 13.69 mm (11,12)	$\lambda_c =$ 12.48mm (13)	$\lambda_c =$ 11.84mm (11)		$\lambda_c =$ 13.04mm (10,11)	$\lambda_c =$ 13.49mm (10)		$\lambda_c =$ 15.50mm (9)	$\lambda_c =$ 16.54mm (10)			$\lambda_c =$ 18.83mm (9)
$\frac{R_L}{R_A} = 1.5$	$\lambda_c =$ 10.92mm	$\lambda_c =$ 22.35mm	$\lambda_c =$ 13.46mm	NW	$\lambda_c =$ 28.70mm	$\lambda_c =$ 18.03mm	NW	NW	$\lambda_c =$ 24.38mm	NW	NW	$\lambda_c =$ 41.91mm
	$\lambda_c =$ 18.49mm (10)	$\lambda_c =$ 15.65mm (13)	$\lambda_c =$ 12.51mm (12)		$\lambda_c =$ 21.05mm (11,12)	$\lambda_c =$ 15.10mm (12)			$\lambda_c =$ 18.70mm (12)			$\lambda_c =$ 40.77mm (10,11)
$\frac{R_L}{R_A} = 1.7$	NW	$\lambda_c =$ 34.80mm	$\lambda_c =$ 22.86mm	NW	$\lambda_c =$ 38.86mm	$\lambda_c =$ 29.46mm	NW	NW	$\lambda_c =$ 36.58mm	NW	NW	$\lambda_c =$ 54.36mm
		$\lambda_c =$ 29.59mm (14)	$\lambda_c =$ 13.95mm (13)		$\lambda_c =$ 32.35mm (12,13)	$\lambda_c =$ 18.31mm (14)			$\lambda_c =$ 33.98mm (12,13)			$\lambda_c =$ 51.60mm (11,12)

(1985)), the results were in agreement with the theoretical predictions. Some of the deformed specimens are depicted in Plate 3.

4 Results and Discussion

Blanks from four different thickness sheets were employed in the experiments, namely $H_1 = 0.508$ mm, $H_2 = 0.635$ mm, $H_3 = 0.813$ mm and $H_4 = 1.016$ mm. For a given set of tools S_i and a given initial sheet thickness H_j three different sets of blanks were considered with radii $R_L = 1.3R_A$, $R_L = 1.5R_A$ and $R_L = 1.7R_A$ with R_A the aperture radius of the blank. In total 36 sets of tests were conducted in order to determine the critical dome height (or punch advance) λ_c at the onset of a puckering instability in each case.

The ring loads, necessary to avoid flange wrinkling during the experiments are presented in Table 2 in the next page.

Although all the possible measures to avoid the friction between the workpiece and the tooling have been taken, some friction is still unavoidable. Guided by strain distribution measurements for axisymmetrically drawn blanks, a best fit between theory and experiment was found for a friction coefficient $\mu = 0.04$. Hence, a friction coefficient $\mu = 0.04$ was adopted for all the subsequent calculations. This value is well within the range of friction coefficients found by Nine (1978) during his draw bead experiments.

The only material characteristics that cannot be directly specified from an experiment are the model's corner characteristics. As discussed repeatedly in the plastic bifurcation literature (see for example Christofferson and Hutchinson (1979), Hutchinson [1974], or Stören and Rice (1975)), in spite of the nonobservability of such a vertex, the deformation theories of plasticity predict successfully the reduction of incremental moduli in load directions approaching proportional loading, and hence they are found useful in modeling plastic buckling.

Various values for the forward loading θ_0 and unloading θ_c angles were tried. The values that were finally adopted for all the calculations presented in this work are $\theta_0 = 0$ and $\theta_c = \pi/2$ and were chosen on the basis that they gave the best experimental/theoretical agreement for the S_3 tooling case $H_4 = 1.016$ mm thickness blanks.

Table 3 presents the experimental, as well as the theoretical results for the critical dome height corresponding to the onset of puckering. The top (shaded) number in every box corresponds to the experimentally measured critical advance λ, and the bottom number is the theoretically computed counterpart, while the integer in parenthesis is the theoretically computed critical wavenumber corresponding to the test case in question. The symbol NW in Table 3 stands for a successful draw with no puckering observed (for a dome height equal to a punch radius R_P).

As seen in Table 3, the biggest discrepancy between the theoretical and experimental results occurs for the thinner sheets and for the lower drawing ratios. This systematic discrepancy (the theory always overestimates the critical height) is due to the crude modeling of the uniaxial stress-strain curve at small strains. As explained in Triantafyllidis (1985), the determining factor for the onset of the puckering instability is reaching a critical level of hoop stress in the unsupported part of the shell. Since for low strains, the bilinear approximation of the uniaxial curve (see Fig. 2) overestimates the strains (for a given stress level), the corresponding theoretical critical height is also going to be overestimated. The discrepancy is aggravated by the fact that at the beginning

of the drawing process, the strains increase less rapidly than at the end.

Since in the present work the bifurcation of the structure well into the plastic range is of primary interest, no effort was made to finetune the model in the small strain regime. An improvement of the present model in this direction is straightforward.

As discussed in detail in Triantafyllidis (1985), the puckering instability problem under investigation, possesses a rather unique feature in the class of plastic bifurcation problems, namely the very strong deviations of the principal solution from the total loading condition in the contact-free part of the sheet. Therefore, the fact that the values of θ_0 and θ_c required for the best correlation between theory and experiment for the case of the instabilities occuring deep in the plastic range of the material's response are $\theta_0 = 0$, $\theta_c = \pi/2$ which correspond to the flow theory model (i.e. the stiffest possible incremental response) is of no surprise.

Moreover, and in view of the presence of strong deviations from proportional loading in the principal solution in that part of the structure, where the eigenmode amplitude is maximized, a smooth bifurcation in the sense of Triantafyllidis (1983), Nguyen and Triantafyllidis (1989) is expected. The fact that the bifurcated branch emanates tangently from the principal one, makes the accurate experimental detection of the onset of bifurcation difficult. It is expected that for bifurcations deep in the plastic range their experimental detection will always be at a higher dome height than the one corresponding to their onset, thus justifying the fact in Table 3 the theoretical predictions in the corresponding cases are slightly lower than the experimental results.

5 Conclusions

As explained in the introduction, the scope of the present experiments is twofold. On the theoretical side, the problem possesses the very interesting feature of strong deviations from proportional loading in its prebuckling solution. This property makes a smooth bifurcation possible and poses difficulties in the experimental determination of the onset of buckling. In order to avoid taking sides in the still unresolved debate of the proper constitutive choice for plastic buckling problems, a constitutive relation was chosen for theoretical calculations that can model all types of incremental behavior from the softest (deformation type) to the stiffest (flow type) theory of plasticity. It is not surprising that, due to the stiffening effect of the large deviations from proportional loading in the principal solution, the best experimental—theoretical fit is chieved when the flow theory of plasticity is employed. This finding is the opposite of what is observed in the vast majority of plastic buckling experiments conducted thus far, and understandably so, in view of their corresponding proportional or near proportional loading prebuckling states.

On the practical side, the present experiment also serves as a simple but realistic model for surface waviness instabilities occuring in complex sheet metal forming operations. By employing an instability criterion which requires only the membrane prebifurcation solution of the structure (and thus avoiding the complication of a full nonlinear shell theory model that classical shell buckling theory would have required) one can achieve a very good agreement between the theory and the experiment. Hence the present experiments provide a good check for the usefulness and accuracy of a general methodology developed in Triantafyllidis and Kwon (1987) for the determination of the onset of surface waviness instabilities in arbitrarily shaped thin walled structures.

Acknowledgments

Support for this work from the General Motors Corporation to The University of Michigan is gratefully acknowledged.

References

1 Devons, J. D., 1941, *The Metallurgy of Deep Drawing and Pressing*, Chapman Hall, London.

2 Triantafyllidis, N., 1983, "On the Bifurcation and Postbifurcation Analysis of Elastic-Plastic Solids Under General Prebifurcation Conditions," *Journal of the Mechanics and Physics of Solids*, Vol. 31, pp. 499–510.

3 Nguyen, S., and Triantafyllidis, N., 1989, "Plastic Bifurcation and Postbifurcation for Generalized Standard Continua," to appear in *Journal of the Mechanics and Physics of Solids*.

4 Triantafyllidis, N., and Kwon, Y. J., 1987, "Thickness Effects on Shell Stability; A General Theory with Applications," University of Michigan Aerospace Engineering Department Report.

5 Triantafyllidis, N., 1985, "Puckering Instability Phenomena in the Hemispherical Cup Test," *Journal of the Mechanics and Physics of Solids*, Vol. 33, pp. 117–139.

6 Triantafyllidis, N., and Maker, N. B., and Samanta, S. K., 1986, "An Analysis of Draw Beads in Sheet Metal Forming Part I—Problem Formulation," JOURNAL OF ENGINEERING MATERIALS AND TECHNOLOGY, Vol. 108, pp. 321–327.

7 Christoffersen, J., and Hutchinson, J. W., 1979, "A Class of Phenomenological Corner Theories of Plasticity," *Journal of the Mechanics and Physics of Solids*, Vol. 27, pp. 465–487.

8 Nine, H. D., 1987, "Drawbead Forces in Sheet Metal Forming," *Mechanics of Sheet Metal Forming*, Plenum Press, New York, pp. 203–211.

9 Hutchinson, J. W., 1974, "Plastic Buckling," *Advances in Applied Mechanics*, edited by C. S. Yih, Vol. 14, pp. 64–144.

10 Stören, S., and Rice, J., 1975, "Localized Necking in Thin Sheets," *Journal of the Mechanics and Physics of Solids*, Vol. 23, pp. 421–441.